Supersonic molecular jet studies of toluene–helium and toluene–methane clusters

Mark Schauer, K. Law, and E. R. Bernstein

Supersonic molecular jet studies of toluene–helium and toluene–methane clusters[a]

Mark Schauer, K. Law, and E. R. Bernstein

Department of Chemistry, Condensed Matter Sciences Laboratory, Colorado State University, Fort Collins, Colorado 80523

The techniques of fluorescence excitation (FE), dispersed emission (DE), and one- and two-color time of flight mass spectroscopy (TOFMS) have been employed to study van der Waals clusters of toluene–helium (TolHe) and toluene–methane (TolCH$_4$) formed in a supersonic molecular jet. Spectral shifts for the toluene $^1B_2\leftarrow{}^1A_1$ transition have been characterized for TolHe$_{1,2}$ and Tol(CH$_4$)$_{1,2}$. The van der Waals stretching frequencies (V^1) in the excited states of these clusters have been identified. The ground state stretch (V_1) for TolHe has also been found; it is quite similar to the TolHe V^1. The binding energies (D_0) for Tol–He clusters lie between 75 and 90 cm^{-1} and those for Tol–CH$_4$ clusters lie between 533 and 739 cm^{-1}. The coordination of a third solvent molecule to those clusters generates a broad spectrum whose shift is close to the limiting value for a large ($x > 3$) cluster. A comparison between these data and methane solution data is presented.

I. INTRODUCTION

A number of recent supersonic molecular jet studies have dealt with the generation and characterization of van der Waals (vdW) molecules formed between a solute species (tetrazine,[1] aniline,[2] benzene,[3] etc.) and small solvent molecules (helium, argon, methane, etc.). Several reports have discussed vdW clusters as model solute/solvent cage systems.[2,4] Previous work from our laboratory[2(a),2(b)] has related the observed spectroscopic properties of vdW clusters with spectroscopic properties of cryogenic liquid solutions.[5] The comparison between gas phase clusters and simple solutions has proved useful: it has shed some light on solute/solvent cage structure and dynamics. Various cluster processes, such as vibrational predissociation (VP) and intramolecular vibrational redistribution (IVR), can be invoked to rationalize the behavior of a solute molecule in solution. Specifically, it has been possible to relate aniline (An) methane cluster data to aniline cryogenic solution behavior.[2(b)]

Toluene (Tol) is perhaps a better solute molecule than An with which to pursue this comparison: liquid state data have already been published from this laboratory[5(a)] dealing with Tol dissolved in several small cryogenic hydrocarbon solvents. Fluorescence excitation (FE) and dispersed emission (DE) spectra of Tol in a molecular jet have already been reported.[6] In addition, the data presented in this paper for Tol should complement that obtained for An, since An and Tol have similar geometries, molecular properties, and interactions with small hydrocarbons.

Two problems arise in the study of Tol vdW clusters in a molecular jet: several low frequency Tol vibrational features have not previously been assigned, and the Tol dimer [Tol$_2$] FE spectrum overlaps with and obscures some of the cluster transitions. Assignments for weak features in the Tol spectrum have to be made in order to understand the major features in the cluster DE spectra. Two-color time of flight mass spectroscopy (2-color TOFMS) studies allow separation of

monomer, cluster, and Tol dimer features quite clearly, as will be shown below.

This paper will present data on Tol–He and Tol–CH$_4$ vdW clusters: the elaborate (Tol)$_x$ ($x = 2,3,4...$) spectra will be treated in a separate publication. The results of our investigations on these two cluster systems will be compared with our previous data for An–He and An–CH$_4$ vdW clusters[2(a),2(b)] and for Tol dissolved in cryogenic liquid solutions.[5(a)] The Results section examines FE, DE, and 1- and 2-color TOFMS spectra for the Tol–He and the Tol–CH$_4$ systems. The Discussion section will focus on the physical properties of the vdW clusters and their dynamical processes. Properties of the Tol–CH$_4$ clusters will be compared with those of aniline–methane clusters and toluene–methane liquid solutions.

II. EXPERIMENTAL PROCEDURES

The supersonic molecular jet apparatus currently employed in this work has been described previously[2(a),2(b)]: laser power and beam conditions are the same as given in these references. All spectra are obtained with low enough power to avoid saturation in both pump and ionization processes. Three different studies are carried out for this work. Fluorescence excitation (FE) experiments monitor the total fluorescence of all species in the beam as the laser wavelength is scanned through the solute absorption region. For a solute species with high quantum yield, the total emission is directly related to absorption. The spectrum thus obtained is proportional to a composite absorption spectrum of all species in the molecular jet. Dispersed emission (DE) spectra are obtained as a particular feature in the FE spectrum is excited and the ensuing emission is resolved with a single grating scanning monochromator. DE spectra can consist of emission features from more than one species in the beam due to overlap of absorption peaks. Laser intensity for both FE and DE experiments is kept well below 2 mJ/pulse to avoid saturation. The most selective experiment for species identification is time of flight mass spectroscopy (TOFMS). Ionization is accomplished selectively by either 1- or 2-color resonance
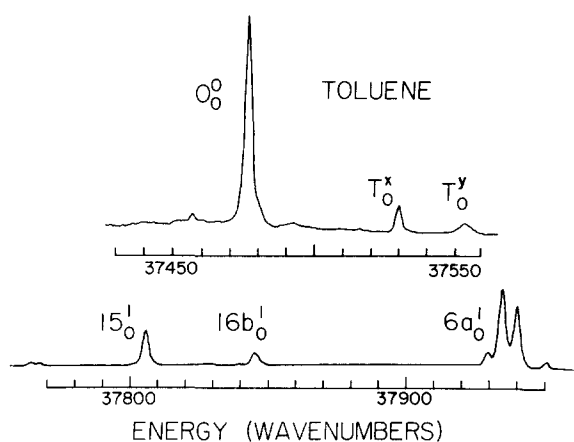

FIG. 1. Portions of the FE spectrum of toluene in the region encompassing Tol 0_0^0 and Tol $6a_0^1$. For this spectrum $P_0 = 150$ psi. Some of the peaks are due to Tol$_2$ species. No TolHe$_x$ peaks are present (see Table I).

enhanced 2 photon ionization. Two detection modes for the TOFMS can be employed: the intensity in a specific mass channel can be monitored as the pump beam is tuned; or, the time base of the TOFMS can be swept to detect all ion masses arriving at the detector for the duration of the experiments. One-color TOFMS is typically more intense than 2-color TOFMS; however, the 2-color excitation does not cause ion fragmentation and, thereby, loss of mass selectivity. In the 2-color TOFMS experiment the pump beam is always maintained at a low intensity ($\sim 100 \,\mu$J/pulse) in order to insure that 1-color TOFMS does not occur. Blocking the ionization beam in the 2-color TOFMS experiment results in no appreciable TOFMS signal. Scanning the wavelength of the pump beam in a 2-color TOFMS experiment and detecting at a particular mass channel results in an absorption spectrum of the particular mass species monitored.

Both cw (25 μm orifice) and pulse (500 μm orifice) nozzles are used with the TOFMS experiments. The pulsed nozzle is advantageous in these experiments because of its large nozzle diameter and low duty cycle. The relative distance between the nozzle and the ionization region of the TOFMS is reduced from 21 320 nozzle diameters for the cw nozzle to 1066 for the pulsed nozzle; this reduction should lead to a

factor of 400 increase in beam density, and thereby signal intensity, at the TOFMS. In practice the signal increase in the Tol mass channel is about a factor of 50 for the pulsed nozzle with respect to the cw nozzle.

Toluene is treated in the same manner as previously described for aniline.[2(a),2(b)] Aldrich spectroscopic grade toluene is used without purification. The carrier gas, either pure helium or a mixture of helium and methane, is passed over liquid toluene in a stainless steel trap at room temperature. The nozzle is also maintained at ambient temperature. The concentration of toluene in the beam varies as a function of the backing pressure (P_0).

III. RESULTS

In order to interpret the toluene van der Waals cluster data, it is quite useful to assign the toluene features in the regions encompassing the Tol 0_0^0 and Tol $6a_0^1$. The tentative assignments suggested here are based on toluene previously published[7] IR spectra and on the aniline electronic spectrum. The lowest frequency peaks observable above the Tol 0_0^0 (Fig. 1 and Table I) have been previously identified as hot bands of the methyl torsion modes.[6(a)] Molecular jet spectra, however, demonstrate that the features at 53 and 76 cm^{-1} are not hot bands, as their intensity relative to the Tol 0_0^0 intensity does not vary over a wide range of backing pressures (50 and 800 psi). These features are labeled T_0^x and T_0^y (x and y denote unknown quanta of this methyl torsional motion in the excited state). The two peaks at 288 and 291 cm^{-1} above the Tol 0_0^0 are assigned as $10b_0^2$ and $16a_0^2$ primarily due to the similarity of these peaks to analogous features in the aniline spectrum. Based on toluene IR data, the bands at 329 and 368 cm^{-1} may be 15_0^1 and $16b_0^1$, respectively. The doubling of the $6a_0^1$ peak in the absorption spectrum of toluene has been attributed to Fermi resonance between $6a^1$ and an unidentified level.[6(b)]

These two regions of the toluene spectrum also contain features that are not associated with free molecular toluene. The peak at -19.7 cm^{-1} relative to the Tol 0_0^0 and a similar peak near $6b_0^1$ are due to absorption of the (Tol)$_2$ species. Preliminary 2-color TOFMS of the Tol dimer reveals a complicated broad structure with a sharp peak at -19.7 cm^{-1}

TABLE I. The toluene FE spectrum in the region encompassing Tol 0_0^0 and Tol $6a_0^1$ (see Fig. 1).

Wavelength (vac Å)	Energy (vac cm^{-1})	Relative energy (cm^{-1})	Assignment	
2669.67	37 457.7	$-$ 19.7	Tol$_2$	0_0^0
2668.26	37 477.5	0		0_0^0
2664.48	37 530.8	53.3		T_0^x
2662.83	37 554.0	76.5		T_0^y
2647.90	37 765.7	288.2		$10b_0^2$
2647.71	37 768.5	291.0		$16a_0^2$
2645.01	37 807.0	329.5		15_0^1
2642.31	37 845.6	368.1		$16b_0^1$
2636.34	37 931.4	453.9	Tol$_2$	$6a_0^1$
2635.97	37 936.7	459.2		$6a_0^1$
2635.73	37 940.1	462.6		$6a_0^1$
2635.04	37 950.1	472.6		?

from the Tol 0_0^0 and intensity on both the high and low energy sides of the Tol 0_0^0. The dimer spectra will be studied more extensively in the near future.

A. Tol–He

The FE spectra of various vibronic bands of the Tol–He system clearly show TolHe$_x$ vdW peaks to the high energy side of the Tol peaks. The 0_0^0 region (Fig. 2) and the $6b_0^1$ region (Fig. 3) evidence similar patterns. TolHe and TolHe$_2$ vibronic features exhibit a small additive blue shift with respect to comparable Tol vibronic transitions: peaks due to Tol–He vdW vibrational additions to these cluster vibronic origins are found further to the blue. The $6a_0^1$ region (Fig. 4) looks qualitatively similar to the 0_0^0 and $6b_0^1$ regions; however, congestion due to the apparent Fermi resonance $6a^1$ makes assignments difficult.

The 2-color TOFMS data for various species in the 0_0^0 region in general confirm the above qualitative identification and generate species specific assignments. Figure 5 presents the 2-color TOFMS for Tol, TolHe, and TolHe$_2$: a small additive successive shift to higher energy is evident between these three origins. In addition, the vdW stretching vibrational mode progression can be uniquely identified (Figs. 5 and 6) for each species. The TolHe$_3$ spectrum is, however, broad and somewhat structured with a nonadditive blue shift.

An expanded trace of the TolHe and TolHe$_2$ 2-color TOFMS (Fig. 6) shows the vdW stretching modes in more detail (see also Table II). The stretching frequency in both species is nearly the same. The stretching progression can be
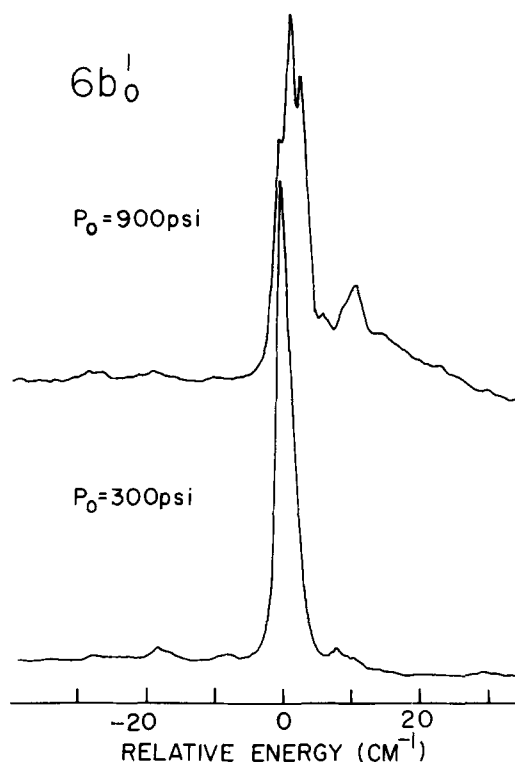
FIG. 3. FE spectra for the $6b_0^1$ region at high (upper trace) and low backing pressures of He. The energy scale is relative to Tol $6b_0^1$ (38 010.5 cm^{-1}). Note the similarity in the pattern of vdW peaks with that found in the 0_0^0 region. Some intensity due to Tol$_2$ species is evident to the red of Tol $6b_0^1$.
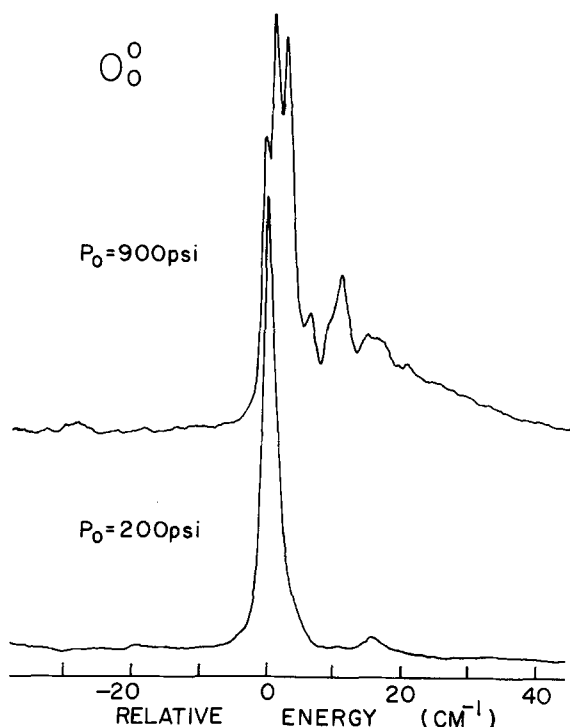
FIG. 2. FE spectrum of toluene expanded in He at high (upper trace) and low backing pressures. The energy scale is relative to Tol 0_0^0 (37 477.5 cm^{-1}). Note the vdW cluster peaks to the blue of the Tol 0_0^0.
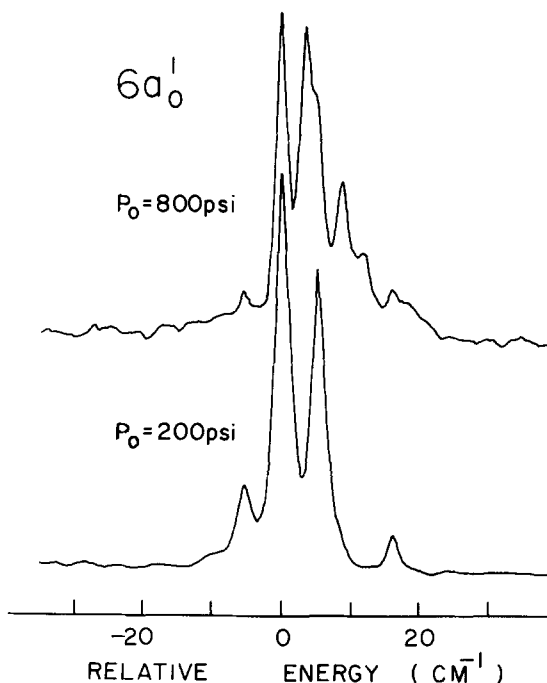
FIG. 4. FE spectra for the $6a_0^1$ region at high (upper trace) and low backing pressures of He. Due to Fermi resonance, the Tol $6a_0^1$ is a doublet. Consequently vdW peaks of the lower energy feature interfere with those of the higher energy feature. Also, intensity due to Tol$_2$ is evident to the low energy side of the Tol $6a_0^1$ transition. The energy scale is relative to the lower energy Tol $6a_0^1$ feature (37 937.5 cm^{-1}).
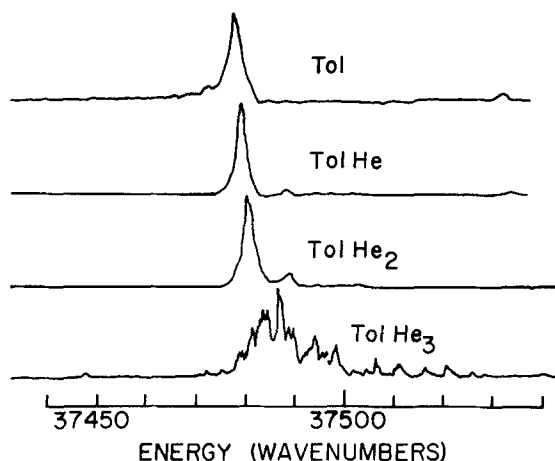
FIG. 5. Two-color TOFMS of Tol and several TolHe$_x$ clusters in the 0_0^0 region. Some fragmentation is evident in the Tol spectra as shown by the presence of some intensity due to Tol$_2$ and TolHe$_x$ features. However in the TolHe$_x$ 2-color TOFMS spectra the pump beam intensity was kept below $\sim 100\,\mu$J/pulse and fragmentation is not evident.

employed to estimate the dissociation energy D_0 by fitting the frequencies to a Morse potential oscillator in the usual fashion: an estimate of $D_0 \sim 30$ cm^{-1} for TolHe obtains. However, this estimate is clearly low. The TolHe 2-color TOFMS contains both the peaks at 53 and 76 cm^{-1} above the TolHe 0_0^0. The TolHe$_2$ species shows evidence of these features as well (see Fig. 6). These observations imply that the D_0 for both species is greater than ~ 76 cm^{-1}.

The dominant features in the DE spectrum of TolHe 0^0 are similar to those in the Tol 0^0 DE spectrum. Under high resolution ($\Delta\nu \sim 5$ cm^{-1}) a short progression in the ground state vdW stretching mode is evident. This feature is presented in Fig. 7. The observation of this short ground state progression emphasized both the similarity of the ground and
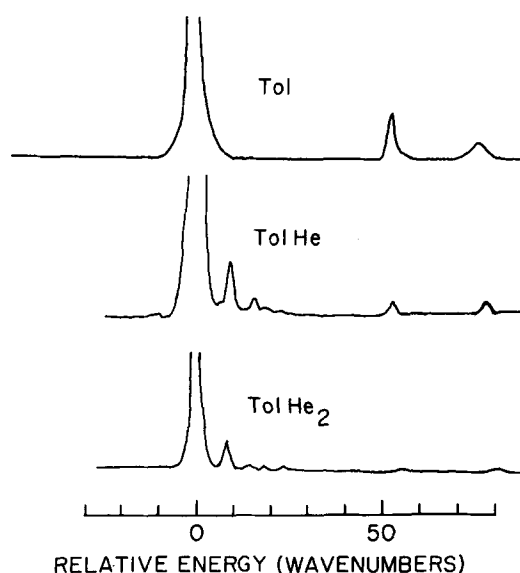

FIG. 6. Expanded 2-color TOFMS of Tol and TolHe$_x$ in the 0_0^0 region. The 0_0^0 peaks have been artificially aligned at 0 relative energy. Note the similarity in the vdW stretch progression for TolHe and TolHe$_2$. Also, note the presence of TolHe T_0^x and T_0^y peaks (see Table II).

excited state stretching vibrations and the strong $\Delta V = 0$ propensity rule for the vdW motion.

Emission arising from the excitation of higher vibronic levels of TolHe is much more complicated than that obtained by pumping the comparable Tol feature. The DE spectrum arising from the TolHe $6a^1$ level is quite congested (see Table III); some of the peaks in this emission can be identified as emission from a number of Tol excited vibronic levels. The relatively small binding energy of TolHe allows vibrational predissociation (VP) to a large number of lower levels of Tol. The intensity of any one distinct feature of the TolHe DE is much less than that of the comparable Tol feature because the total emission intensity is spread out over so many transitions. The emission found by pumping TolHe $6b^1$ is very similar to that found for $6a^1$. These data are summarized in Table IV. The presence of Tol $6a^1$ emission in this latter spectrum suggests that 73 cm^{-1}, the difference in energy between the $6b^1$ and $6a^1$ levels, may be enough energy to cause VP of the TolHe vdW complex. This would set an upper limit to the D_0 for TolHe of roughly 73 cm^{-1}. This value and the apparent contradiction with the lower limit found above, will be discussed further in the next section.

B. Tol–CH$_4$

The Tol–CH$_4$ spectra appear to the low energy side of the comparable Tol vibronic features. The TolCH$_4$ 0_0^0 is shift -43 cm^{-1} from the Tol 0_0^0 and several vdW mode features can be identified between the TolCH$_4$ and Tol 0_0^0 transitions (see Fig. 8). Tentative assignments can be made for the vdW features and they are presented in Table V. Tol(CH$_4$)$_2$ exhibits an additive spectral shift for the 0_0^0 feature and a slightly more complicated set of vdW peaks. A vdW stretching progression similar to the one characterized for TolCH$_4$ is evident in addition to comparable bending modes. A relatively intense feature at Tol(CH$_4$)$_2$ $0_0^0 + 63$ cm^{-1} can be tentatively assigned as either the independent stretching of both TolCH$_4$ bonds (a harmonic "double" excitation) or a second Tol(CH$_4$)$_2$ 0_0^0 for another configuration.

Larger clusters also absorb in this region as shown in Fig. 9. If the region between the Tol(CH$_4$)$_2$ 0_0^0 and 50 cm^{-1} to the low energy side of this feature is pumped, Tol(CH$_4$)$_x$ ($3 < x < 15$) clusters and Tol$_n$(CH$_4$)$_x$ ($n = 2,3,4,...$ and $x = 1,2,3,...$) clusters are observed. Preliminary absorption spectra of some of these species reveal complicated structures; these spectra will be the subject of a future publication.

Higher vibronic transitions of Tol(CH$_4$)$_x$ evidence spectra that are quite similar to those just described for the 0_0^0 region. FE spectra of the $6a_0^1$ and $6b_0^1$ regions show patterns of TolCH$_4$ and Tol peaks that are nearly identical in appearance to the spectra of Fig. 8. The TolCH$_4$ vibronic bands are red shifted 43 cm^{-1} from their respective Tol counterparts and vdW vibrational features are evident to the high energy side of the TolCH$_4$ vibronic origins. The Tol–CH$_4$ species also generate 2-color TOFMS in the $6a_0^1$ and $6b_0^1$ regions. This indicates that the $6b^1$ vibrational energy (533 cm^{-1}) is insufficient to cause vibrational predissociation of the TolCH$_4$ vdW cluster on the time scale of the experiment.[8] Since the TolCH$_4$ 1_0^1 transition is not observed

TABLE II. TolHe and TolHe$_2$ 2-color TOFMS in the 0_0^0 region (see Fig. 6).

	Energy (vać cm^{-1})	Relative energy (cm^{-1})	Assignment[a]
TolHe (1.55 cm^{-1} relative to Tol 0_0^0)			
	37 479.1	0	TolHe 0_0^0
	37 488.2	9.1	TolHe V_0^1
	37 494.6	15.5	TolHe V_0^2
TolHe$_2$(3.18 cm^{-1} relative to Tol 0_0^0)			
	37 480.7	0	TolHe$_2$ 0_0^0
	37 489.5	8.85	TolHe$_2$ V_0^1
	37 495.4	14.7	TolHe$_2$ V_0^2

[a] V refers to the vdW stretching mode.

with 2-color TOFMS detection, the dissociation energy for the vdW cluster can be bracketed between 533 and 739 cm^{-1}. Of course, FE spectra for Tol–CH$_4$ can be observed to much higher vibronic energies.

The TolCH$_4$ DE spectra are weak and much more congested than comparable Tol spectra. The TolCH$_4$ 0^0 DE spectrum evidences some weak features similar to those found in the Tol 0_0^0 DE spectrum; however, a large background of unassignable features is also present. A parallel set of spectra obtain for the TolCH$_4$ $6a^1$ DE. The TolCH$_4$ 1^1 DE spectra consists only of Tol 0_0^0 emission peaks, demonstrating that at this energy (733 cm^{-1}) the TolCH$_4$ undergoes vibrational predissociation on the time scale of the fluorescence lifetime ($\sim$70 ns). Even at this energy, however, a broad background of unassignable intensity is evident; the low intensity and broad background seem generally to characterize the Tol(CH$_4$)$_x$ emission.
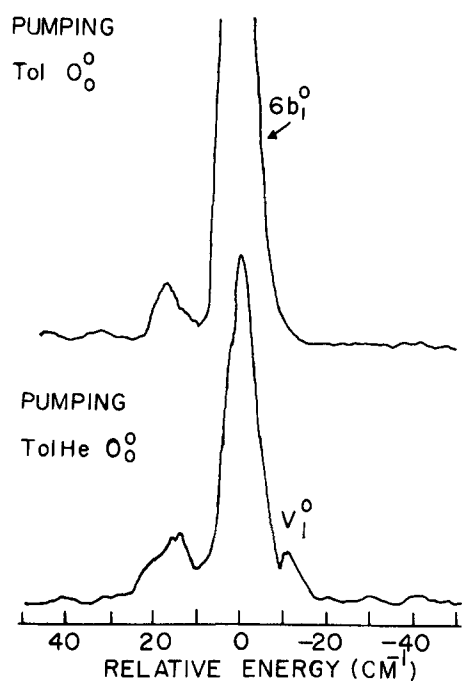

PUMPING
Tol 0_0^0

$6b_1^0$

PUMPING
TolHe 0_0^0

V_1^0

|_____|_____|_____|_____|_____|
  40   20   0   -20   -40
      RELATIVE ENERGY (CM^{-1})

FIG. 7. Part of the high resolution DE spectrum of Tol 0^0 and TolHe 0^0. The feature at -18 cm^{-1} relative to the main peak in both spectra is due to Tol$_2$. The energy scale is relative to Tol $6b_1^0$. Note the V_1^0 peak which gives the energy of a vdW mode in the ground state.

IV. DISCUSSION

In this section a more in depth treatment of cluster geometry, solvent spectral shift, binding energy, and the comparison between solution and cluster properties will be presented. First, however, a few general remarks on the spectra are in order.

While the signal to noise ratio for the FE and 2-color TOFMS Tol cluster experiments is quite reasonable and roughly comparable to those for aniline clusters, the DE spectra are generally quite congested and low in intensity. We attribute this to four causes: (1) the overall emission intensity from toluene and toluene clusters appears relatively low due to the long lifetime of the fluorescence ($\sim$70 ns); (2) concentration of the clusters in the beam is kept low to optimize the spectral resolution of small cluster features; (3) VP seems to occur to a large number of lower vibronic levels of toluene; and (4) some of the emission is associated with (Tol)$_x$ and (Tol)$_x$(solvent)$_y$ whose absorption overlaps that of the clusters. The latter point is not trivial because the beam conditions which apparently favor vdW clusters (P_0 200 psi, room temperature toluene and nozzle) also seem to produce a substantial concentration of (Tol)$_x$ complexes.

Because of the poor quality of the DE spectra, it has not been possible thus far to characterize the intramolecular vibrational relaxation (IVR) processes for Tol–He or Tol–CH$_4$ cluster. It is clear, however, that the IVR process is important for this system; at levels for which VP occurs, a much cleaner, more intense DE spectrum obtains. The characteristic times for the various processes—VP, IVR, second photon absorption, fluorescence—appear to be of the same order as found for the aniline cluster system.[8] Thus, VP is slower than 5 ps, IVR times lie between VP and fluorescence times, and the time taken to absorb the ionizing photon is longer than the VP time but shorter than the IVR time.

The last general point to be made concerning the Tol and Tol cluster spectra is derived from the 2-color TOFMS. The ionization beam energy set by the Tol 0_0^0 is not optimum for any of the Tol vibronic bands nor any of the Tol–CH$_4$ cluster bands. For the Tol vibronic features the ionization energy must be increased by about 100 cm^{-1} over the value predicted based on the Tol 0_0^0 ionization energy in order to maximize the 2-color TOFMS signal. The results for Tol CH$_4$ clusters are similar but not as dramatic. Much larger reductions in the optimum ionization energy are found for

TABLE III. DE spectrum obtained as TolHe $6a_0^1$ is pumped. Only the prominent peaks in the spectrum are reported.

Wavelength (vac Å)	Energy (vac cm^{-1})	Energy relative to Tol 0_0^0 (cm^{-1})	Calculated relative energy (cm^{-1})	Assignment[a]
2668.4	37 475	2	0	0_0^0
2668.7	37 470	7	14	15_1^1
2672.7	37 415	62	62	$6a_1^1$
2674.6	37 388	89	96	$16b_1^1$
2675.6	37 375	103	104	$15_0^1 10b_2^0$
2677.4	37 350	127	120	$10b_0^2 16a_1^0$
2678.7	37 331	146	146	$10b_2^2$
2679.3	37 324	154	153	$16b_0^1 6a_1^0$
2680.7	37 303	175	173	$16a_0^2 16b_1^0$
2681.2	37 297	181	176	$10b_0^2 16b_1^0$
2683.4	37 266	211		$6a_0^1 X_1^0$
2685.1	37 243	234	233	$10b_0^2 6a_1^0$

[a] All fluorescence seems to originate from Tol monomer. X denotes an unknown level in the ground state.

other toluene based systems (i.e., $(Tol)_x$, $Tol-C_2H_6$, and $Tol-C_3H_8$).[9] Comparable data obtain for the aniline clusters studied thus far.[2(a),2(b)] These ionization energy changes have important consequences for 2-color TOFMS signal intensities and are, of course, important for the reduction of ion fragmentation.

A. Geometry

The geometry of the Tol–He and Tol–CH$_4$ vdW clusters can be reasonably well established based on calculations for other aromatic systems,[4(a)] spectral shift data for both toluene and aniline[2] clusters, and by analogy with other systems for which rotational spectra have been obtained.[1,3] For the tetrazine–He and tetrazine–Ar[1] clusters the rare gas atoms have been definitively demonstrated to bind above and below the aromatic ring such as to preserve the symmetry axis perpendicular to the plane; calculations indicate a similar structure for more general ring systems.[4(a)] For binding symmetrically in this manner, additive spectral shifts for the first two ligands are found. Thus, as we have concluded previously for An–He and An–CH$_4$, the first two ligands in

Tol–He and Tol–CH$_4$ clusters add symmetrically above and below the plane of the ring. Clusters involving three ligand (either He and CH$_4$) around aniline or toluene yield absorption spectra very different from those associated with the smaller clusters. In particular, the clusters with three solvent molecules exhibit nonadditive spectral shifts and their spectra contain at least one component which is broad and featureless. This points to the addition of the third ligand to a site perhaps less localized and inequivalent to the sites occupied by the first two ligands. The general properties and geometries of Tol(CH$_4$)$_x$ $(x \geqslant 3)$ clusters present a rather complicated set of problems, however, and will be the subject of future reports from this laboratory.

B. Solvent spectral shift

While cluster geometry is typically controlled by repulsive interactions (proportional to $1/r^{12}$), interactions which generate the binding are associated with the dispersion or polarizability interaction (proportional to $1/r^6$).[4(a)] Changes in these latter interactions upon excitation gives rise to solvent spectral shifts. The observed shifts should therefore

TABLE IV. DE spectrum obtained as TolHe $6b_0^1$ is pumped. Only the prominent peaks in the spectrum are reported.

Wavelength (vac Å)	Energy (vac cm^{-1})	Energy relative to Tol 0_0^0 (cm^{-1})	Calculated relative energy (cm^{-1})	Assignment[a]
2668.3	37 477	0	0	0_0^0
2669.4	37 462	16	14	15_1^1
2673.2	37 409	69	62	$6a_1^1 (16b_0^1 10b_2^0)$
2674.3	37 393	84	78	$15_0^1 16a_1^0$
2675.6	37 375	103	104	$15_0^1 10b_2^0$
2679.1	37 326	151	146	$10b_2^2$
2679.5	37 321	156	153	$16b_0^1 6a_1^0$
2681.1	37 298	179	176	$10b_0^2 16b_1^0$
2683.2	37 269	209		$6a_0^1 X_1^0$
2685.3	37 240	237	233	$10b_0^2 6a_1^0$

[a] All fluorescence seems to originate from the Tol monomer. X denotes an unknown level in the ground state.
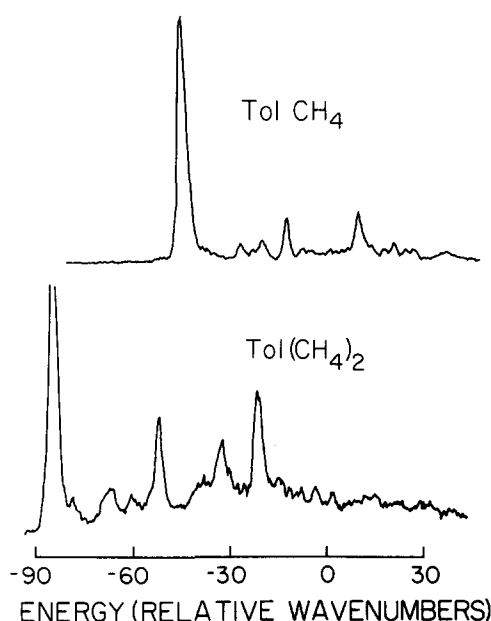
FIG. 8. Two-color TOFMS of TolCH$_4$ (upper trace) and Tol(CH$_4$)$_2$ in the 0_0^0 region. The energy scale is relative to Tol 0_0^0 (37 477.5 cm^{-1}). Note the peaks due to vdW stretches and bends. Tentative assignments are given in Table V.

FIG. 9. One-color TOFMS of Tol(CH$_4$)$_x$ clusters which absorb in the region of the Tol(CH$_4$)$_2$ 0_0^0. The upper trace identifies the species which absorb at the Tol(CH$_4$)$_2$ 0_0^0 position (37 394.5 cm^{-1}). The intensity in the Tol and TolCH$_4$ mass channels is due to fragmentation of larger ions. The lower trace identifies the species which absorb to the red of Tol(CH$_4$)$_2$ (37 370 cm^{-1}); the intensity in the Tol, TolCH$_4$, and Tol(CH$_4$)$_2$ mass channels is due to fragmentation of larger ions. Note the presence of Tol$_2$(CH$_4$)$_y$ clusters and very large Tol$_x$(CH$_4$)$_y$ clusters.

scale with the solvent polarizability and changes in the solute polarizability upon excitation. Thus, aniline–methane and toluene–methane clusters have similar binding energies (nearly the same polarizabilities) but the aniline–methane clusters have a factor of 2 larger solvent shift. As we will report in future papers,[9] however, the (red) shift magnitude is not simply a function of polarizability; it depends essentially on cluster geometry, solute/solvent interaction details, and on the proximity of other solvent molecules.

Helium seems to be an anomalous solvent system, in general; its polarizability is so small that other interactions, perhaps exchange, dominate the energetics of He–solute vdW complexes. Solvent shifts for the Tol–He system are
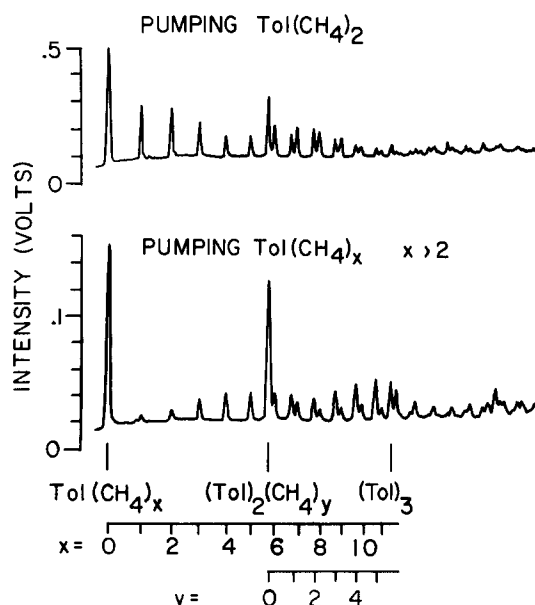
slightly positive (1–3 cm^{-1}) and additive for the first two He atoms. No correlation is obvious between the properties of aniline and toluene and either the size or direction of the He solvent spectral shift; the aniline He shift is slightly negative (1–3 cm^{-1}) with respect to aniline monomer peaks for the first two atoms.[2] Whatever the nature of the He-solute interactions, it changes little upon solute excitation.

The solvent spectral shifts for larger clusters, Tol (solvent)$_x$ $x > 3$, are not additive and are in general quite dependent on the geometry of the particular cluster involved.[9] For these larger clusters certain geometries, at present not well

TABLE V. Two color TOFMS of TolCH$_4$ and Tol(CH$_4$)$_2$ in the 0_0^0 region. Only the prominent peaks are tabulated and tentative assignments are given (see Fig. 8).

Energy (vac cm^{-1})	Relative energy (cm^{-1})	Assignment[a]
TolCH$_4$ ($-$ 43 cm^{-1} relative to Tol 0_0^0)		
37 434.4	0	TolCH$_4$ 0_0^0
37 451.8	17	TolCH$_4$ A_0^1
37 458.7	24	TolCH$_4$ B_0^1
37 466.2	32	TolCH$_4$ V_0^1
37 488.5	54	TolCH$_4$ V_0^2
Tol(CH$_4$)$_2$ ($-$ 83 cm^{-1} relative to Tol 0_0^0)		
37 394.1	0	Tol(CH$_4$)$_2$ 0_0^0
37412.6	18	Tol(CH$_4$)$_2$ A_0^1
37 418.5	24	Tol(CH$_4$)$_2$ B_0^1
37 426.7	32	Tol(CH$_4$)$_2$ V_0^1
37 440.5	46	Tol(CH$_4$)$_2$ $V_0^1 A_0^1$
37 446.2	52	Tol(CH$_4$)$_2$ V_0^2
37 456.9	63	Tol(CH$_4$)$_2$

[a] Tentative assignments are as follows: V stands for the Tol–CH$_4$ stretch, and A and B are different vdW bends. The feature at Tol(CH$_4$)$_2$ 0_0^0 + 63 cm^{-1} can be assigned as either a simultaneous double excitation of independent stretches of both Tol–CH$_4$ bonds or the 0_0^0 of a new configuration of Tol(CH$_4$)$_2$.

characterized, possess shifts that converge around -150 cm^{-1}. This latter shift is quite comparable to the gas to liquid shift (-177 cm^{-1}) reported for a toluene–methane solution[5(a)]; in fact, the two values are certainly identical within experimental resolution.

C. Binding energy

The binding energy for Tol–He can be found in two different experiments; 2-color TOFMS and DE from high vibronic levels. The 2-color TOFMS for the 76 cm^{-1} methyl motion in the excited state sets a lower limit to the binding energy; that is, $D_0 > 76$ cm^{-1}. Although the DE spectra from TolHe $6a^1$ and $6b^1$ are quite weak and the important regions are highly congested, the prominent features in the spectra can be assigned (see Tables III and IV). Several emission features in the TolHe $6a^1$ DE spectrum are identified as originating from Tol 15^1: a firm upper limit of 91 cm^{-1}, based on the $6a^1$–15^1 energy gap, can thus be set for the binding energy. In addition, the weak, congested emission from TolHe $6b^1$ appears to contain features originating from Tol $6a^1$. Although the assignments are less certain in this instance, the observations of Tol $6a^1$ emission would suggest an upper limit of 73 cm^{-1} (the $6b^1$–$6a^1$ energy separation) to the binding energy. While this upper limit seems in conflict with the 2-color TOFMS derived lower limit of 76 cm^{-1}, a number of kinetic processes could be invoked to rationalize the apparent difficulty. A value of the Tol–He $D_0 \sim 75$ cm^{-1} is not unreasonable but it is probably best to suggest that $75 \leqslant D_0 \leqslant 90$ cm^{-1}.

Note that this binding energy is approximately one-half of that found for aniline–He. However, the polarizabilities of aniline and toluene are both $11 \pm 10\%$ Å^3 in the ground state[10]; the ground and excited state binding energy are expected to be nearly identical based on the small spectral shifts.

The binding energy for Tol–CH$_4$ is indistinguishable from that of aniline–CH$_4$; D_0 lies between 533 and 739 cm^{-1}. The correlation between polarizability and binding energy should not be extrapolated to other systems; however, it does not hold, for example, for toluene solvated by ethane and propane for which detailed structure and geometry can produce nearly a factor of 2 change in the binding energy.[9]

D. Solution properties

Parallels between solution properties and cluster spectral shifts, binding energies, and dynamics (VP and IVR) have already been mentioned in our previous publications.[2(a),2(b)] The new information derived from the Tol–CH$_4$ system concerns the trends in the absorption spectra as larger clusters are probed. From TolCH$_4$ and Tol(CH$_4$)$_2$ spectra it is clear that the Tol–CH$_4$ liquid shift of -177 cm^{-1} [5(a)] is rapidly approached by the clusters. This trend seems to be continued by at least a component of the Tol(CH$_4$)$_3$ spectrum. Furthermore, the ubiquitous presence of intensity in the Tol(CH$_4$)$_3$ mass channel as the laser is tuned throughout this region attests to the diffuse nature of this absorption. Such a diffuse absorption is also a characteristic of the solution spectrum. From these observations it seems clear that at least one geometry of the Tol(CH$_4$)$_3$ species is approaching solutionlike properties.

V. CONCLUSIONS

The following Table VI summarizes the data (in cm^{-1}) for the toluene–helium and toluene–methane clusters:

TABLE VI.

Species	Solvent shift	Stretching frequency		Binding energies
		V_1	V^1	
TolHe	1.5	11	9.0	75–90
TolHe$_2$	3.0		8.8	
TolCH$_4$	-43		31.8	533–739
Tol(CH$_4$)$_2$	-83		32.5	

For the Tol–He and Tol–CH$_4$ clusters the first two ligands add above and below the plane of the aromatic ring. The third ligand is suggested to bind in the plane of the ring, probably near the CH$_3$ group. Three coordinated CH$_4$ solvent molecules appear to generate spectral shifts and linewidths similar to those found for toluene–methane solutions. TolHe$_3$ also generates a broad spectrum, shifted only slightly from TolHe$_2$; higher mass clusters fall within the TolHe$_3$ spectrum.

Studies of toluene and aniline solvated by ethane and propane are now in progress; the results will be reported in the near future. Based on these studies, however, caution should be exercised in drawing general conclusions concerning the nature and strength of the interactions, binding energies, and solvent spectral shifts if information on detailed cluster structure is not available. Calculations are also in progress which should generate an assessment of cluster structure and its effect on binding energy, solvent shift, and transition linewidth.

[1](a) R. E. Smalley, L. Wharton, D. H. Levy, and D. W. Chandler, J. Chem. Phys. **68**, 2487 (1978); (b) D. V. Brumbaugh, J. E. Kenny, and D. H. Levy, *ibid.* **78**, 3415 (1983).

[2](a) E. R. Bernstein, K. Law, and Mark Schauer, J. Chem. Phys. **80**, 207 (1984); *ibid.* **80**, 634 (1984); (c) A. Amirav, U. Even, J. Jortner, and B. Dick, Mol. Phys. **49**, 899 (1983).

[3](a) S. M. Beck, M. G. Liverman, D. L. Monts, and R. E. Smalley, J. Chem. Phys. **70**, 232 (1979); (b) K. H. Fung, W. E. Henke, T. R. Hays, H. L. Selzle, and E. W. Schlag, J. Phys. Chem. **85**, 3560 (1981).

[4](a) M. J. Ondrechen, Z. Berkovitch-Yellin, and J. Jortner, J. Am. Chem. Soc. **103**, 6586 (1981); (b) A. Amirav, U. Even, and J. Jortner, J. Chem. Phys. **75**, 2489 (1981); (c) A. W. Castleman, Jr., B. D. Kay, V. Hermann, P. M. Holland, and T. D. Mark, Surf. Sci. **106**, 179 (1981); (d) K. L. Saenger, G. M. McClelland, and D. R. Herschbach, J. Phys. Chem. **85**, 3333 (1981); (e) T. R. Hays, W. Henke, H. L. Selzle, and E. W. Schlag, Chem. Phys. Lett. **77**, 19 (1981); (f) P. M. Felker and A. H. Zewail, *ibid.* **94**, 454 (1983).

[5](a) J. Lee, F. Li, and E. R. Bernstein, J. Phys. Chem. **87**, 1180 (1983); (b) *ibid.* **87**, 1175 (1983); (c) F. Li, J. Lee, and E. R. Bernstein, *ibid.* **87**, 254 (1983); (d) J. Lee, F. Li, and E. R. Bernstein, *ibid.* **87**, 260 (1983); (e) F. Li, J. Lee, and E. R. Bernstein, *ibid.* **86**, 3606 (1982); (f) M. W. Schauer, J. Lee, and E. R. Bernstein, J. Chem. Phys. **76**, 2773 (1982); (g) E. R. Bernstein and J. Lee, *ibid.* **74**, 3159 (1981).

[6](a) J. Murakami, M. Ito, and K. Kaya, Chem. Phys. Lett. **80**, 203 (1981); (b) J. B. Hopkins, D. E. Powers, and R. E. Smalley, J. Chem. Phys. **72**, 5039 (1980); (c) J. B. Hopkins, D. E. Powers, S. Mukamel, and R. E. Smalley, *ibid.* **72**, 5049 (1980).

[7]G. Varsanyi, *Assignments for Vibrational Spectra of Seven Hundred Benzene Derivatives* (Wiley and Sons, New York, 1974).

[8]For further discussion of the time scale of various energy dissipation pathways, see Ref. 2b.

[9]E. R. Bernstein, K. Law, and Mark Schauer (unpublished results).

[10](a) A. K. Burnham and T. D. Gierke, J. Chem. Phys. **73**, 4822 (1980); (b) R. J. W. LeFevre and L. Radom, J. Chem. Soc. B **1967**, 1295; (c) M. Aroney and R. J. W. LeFevre, *ibid.* **1960**, 2161.